Selection of an ASIC1a-blocking combinatorial antibody that protects cells from ischemic death

Min Qiang[a,1], Xue Dong[a,b,c,d,1], Zhao Zha[a], Xiao-Kun Zuo[e,f], Xing-Lei Song[e], Lixia Zhao[a], Chao Yuan[a], Chen Huang[e], Pingdong Tao[a,b,c,d], Qin Hu[e], Wei-Guang Li[e], Wanhui Hu[g], Jie Li[a,b,c,d], Yan Nie[a], Damiano Buratto[a], Francesco Zonta[a], Peixiang Ma[a], Zheng Yu[a,b,c,d], Lili Liu[a], Yi Zhang[a], Bei Yang[a], Jia Xie[h], Tian-Le Xu[e], Zhihu Qu[a,2], Guang Yang[a,2], and Richard A. Lerner[a,h,2]

[a]Shanghai Institute for Advanced Immunochemical Studies, ShanghaiTech University, 201210 Shanghai, China; [b]School of Life Science and Technology, ShanghaiTech University, 201210 Shanghai, China; [c]Institute of Biochemistry and Cell Biology, Shanghai Institutes for Biological Sciences, Chinese Academy of Sciences, 200031 Shanghai, China; [d]University of Chinese Academy of Sciences, 100049 Beijing, China; [e]Collaborative Innovation Center for Brain Science, Department of Anatomy and Physiology, Shanghai Jiao Tong University School of Medicine, 200025 Shanghai, China; [f]Department of Neurosurgery, Affiliated Haikou Hospital, Xiangya Medical College of Central South University, 570100 Haikou, China; [g]iHuman Institute, ShanghaiTech University, 201210 Shanghai, China; and [h]Department of Chemistry, Scripps Research Institute, La Jolla, CA 92037

Acid-sensing ion channels (ASICs) have emerged as important, albeit challenging therapeutic targets for pain, stroke, etc. One approach to developing therapeutic agents could involve the generation of functional antibodies against these channels. To select such antibodies, we used channels assembled in nanodiscs, such that the target ASIC1a has a configuration as close as possible to its natural state in the plasma membrane. This methodology allowed selection of functional antibodies that inhibit acid-induced opening of the channel in a dose-dependent way. In addition to regulation of pH, these antibodies block the transport of cations, including calcium, thereby preventing acid-induced cell death in vitro and in vivo. As proof of concept for the use of these antibodies to modulate ion channels in vivo, we showed that they potently protect brain cells from death after an ischemic stroke. Thus, the methodology described here should be general, thereby allowing selection of antibodies to other important ASICs, such as those involved in pain, neurodegeneration, and other conditions.

antibody | ASIC1a | stroke | neuroprotection | complex structure

Acid-sensing ion channels (ASICs) are voltage-insensitive cation channels belonging to the degenerins/epithelial Na^+ channel superfamily of ion channels (1, 2). In vertebrates, there appears to be at least five ASIC isoforms (ASIC1–ASIC5). Several splicing variants have also been identified for ASIC1 (a and b), ASIC2 (a and b) in rodents and humans, and ASIC3 (a–c) in humans (2). The ASIC proteins consist of a large extracellular domain (ECD), two helical transmembrane domains, and intracellular N and C termini (3). Different ASIC isoforms and splicing variants can combine to form different functional homomeric or heteromeric ASICs on the cell membrane. As the primary acid sensors in responding to extracellular pH perturbation, ASICs are widely distributed in central and peripheral nervous systems throughout the body (4). They are highly expressed in neuronal and nonneuronal cells to ensure normal cellular functions via precisely gauging the acidic microenvironment of each individual cell (5). In the nervous system, ASICs on different sensory cells have been implicated in nociception, mechanosensation, and taste transduction, whereas outside the nervous system, functions of these channels are less understood (4).

Under normal physiological conditions, the extracellular pH is tightly controlled and maintained at around 7.4 (6). Extracellular acidosis results in a sustained decrease in the extracellular pH, a process always accompanied by underlying pathology (7).

In the CNS, ASICs are involved in the synaptic plasticity, learning, and memory (8–10). Brain injury that occurs in inflammation and stroke results in local tissue acidosis and the activation of ASICs (11, 12). The key ASIC protein activated in neuronal injury was shown to be the ASIC1a subtype (11, 13). This subtype has a higher sensitivity to protons and appears to be both sodium and calcium

permeable (14). During severe ischemic stroke, deprivation of oxygen due to the reduction of blood flow increases anaerobic metabolism, leading to the accumulation of lactic acid outside the cells (15). Buildup of lactic acid and H^+ release from ATP hydrolysis induce a drastic decrease in the extracellular pH value (i.e., pH 6.0) (15). In addition to extracellular acidosis, transient increase of calcium induced by the opening of the channel is a trigger that sets in motion still unknown processes that initiate neuronal damage (11). It is often overlooked that ASIC1a also has higher proton permeability than sodium when activated (1), and that the proton influx during acidosis may also induce cell death. The Ca^{2+}-permeable ASIC1a (and its activation), thus, represents a therapeutic target in neuronal injury (16, 17).

The activity of ASICs is known to be regulated by different mechanisms, such as induction of steady-state desensitization (SSD), stabilization of the closed state, and blockage of the channel pore, etc. Multiple ASICs modulators have been identified, including divalent and trivalent ions (18); small drug molecules, such as amiloride (1, 19) and nonsteroidal antiinflammatory drugs (20, 21); the

Significance

Unfortunately, the need for ideal medical treatment of acute ischemic stroke is still largely unmet. One of the contributing factors to the deleterious neuronal death is the opening of acid-sensing ion channels (ASICs) at reduced pH, which in turn, activates other calcium-permeable channels that initiate the catastrophic cascade. Here, we report the discovery of an antibody that blocks the ASIC1a with high specificity and potency. Infusion of this antibody reduces the damaged area from brain ischemia in the murine stroke model. We hypothesize that using antibodies to target ASIC1a is a valid approach for future stroke therapy. The antibody that we report here has the potential to be further developed as drug candidate.

APPLIED BIOLOGICAL SCIENCES

mammalian neuropeptides (RFmide family) (22); endogenous cationic polyamines, such as spermine (23, 24); and venom peptides, such as PcTx1 (25), APETx2 (26), mambalgins (27), MitTx (28), and Hi1a (29). These venom peptides seem to be the most potent and subtype-selective ASICs modulators identified so far (5). However, animal venom peptides, despite their high potency and selectivity, are biologically unstable in humans. Thus, given their general importance, there is a growing demand to identify novel ASIC modulators with greater potency, subtype selectivity, and biological stability. Herein, we use the combinatorial antibody library approach (30–32) to select an antibody that is a highly potent and functional inhibitor of the ASIC1a subtype channel.

We applied a "differential enrichment" strategy using a soluble nanodisc assembly containing a recombinant truncated human acid-sensing ion channel 1a (ΔhASIC1a; 13–464 amino acids). Monoclonal antibodies specific to the ΔhASIC1a were enriched and selected from a single-chain Fv (scFv) antibody library in phage containing 10^{11} members. One antibody, ASC06, showed potent, sustained, and highly selective ASIC1a antagonist activity and protected cells from acid-induced death. In a mouse middle cerebral artery occlusion (MCAO)-induced ischemia stroke model, ASC06 also significantly reduced the infarct size 2 h after stroke, showing a strong neuroprotective effect.

Results

Selection of Functional Antibodies Against *h*ASIC1a Using Nanodiscs.
Removal of the residues at the N- and C-terminal domains (amino acids 1–12 and 465–528, respectively) of *h*ASIC1a has been shown to significantly increase the functional protein expression of *h*ASIC1a (33). We overexpressed and purified the truncated ASIC1a (amino acids 13–464; ΔhASIC1a) to assemble a soluble *h*ASIC1a-displaying system. Nanodiscs were used to mimic the native-like membrane environment and keep the natural extracellular conformation of *h*ASIC1a. The ΔhASIC1a-loaded nanodisc (ΔhASIC1a nanodisc) was further purified on Superose 6 size exclusion chromatography (SEC). Then, the composition of ΔhASIC1a nanodisc was analyzed using SDS/PAGE (*SI Appendix*, Fig. S1*A*). Densitometric analysis of the SDS/PAGE bands corresponding to membrane scaffold protein 1 (MSP1) and monomer ΔhASIC1a revealed that the molar ratio of MSP1 and ΔhASIC1a is ~2:3 (*SI Appendix*, Fig. S1*A*). The homogeneity and diameter of the ΔhASIC1a nanodiscs were further confirmed by dynamic light scattering (*SI Appendix*, Fig. S1*B*). The apparent diameter of the assembled nanodiscs is about 15.5 nm, larger than that of the empty nanodiscs (*ca.* 0.10 nm) and consistent with the incorporation of the ΔhASIC1a proteins in nanodiscs. In accordance, the largest distance in the computation model of the ΔhASIC1a nanodisc is ~14.8 nm, which is from the ECDs to the nanodisc (*SI Appendix*, Fig. S1*B*). Both the ΔhASIC1a nanodiscs and the empty nanodiscs were biotinylated for selections against the combinatorial antibody phage library.

Streptavidin-coated magnetic beads combined with the biotinylated nanodiscs were used in the panning of a human scFv combinatorial antibody library in phage containing 10^{11} members. To minimize the nonspecific interactions of the phagemids with the nanodisc structure, a differential enrichment strategy using empty nanodiscs was used as described in *Materials and Methods*. In *SI Appendix*, Fig. S1*C*, the comparison of the ELISA signals for the control and the antigen-specific nanodisc targets after three rounds of selection is shown. A significant increase in the ELISA signal was observed in the ΔhASIC1a nanodisc group, indicating an enrichment of the scFv antibodies specific to the ΔhASIC1a component of the nanodiscs.

Biophysical Characterization of the Selected Antibodies.
Sequencing of the phagemids collected from the ΔhASIC1a nanodisc group after the third round of selection identified six highly repetitive sequences. The corresponding scFvs were expressed and purified

as a fusion antibody containing the Fc domain of human IgG1. The six scFv-Fc antibodies (molecular mass ~55 kDa in reduced form) were purified and analyzed by SDS/PAGE. As shown in *SI Appendix*, Fig. S1*D*, all six (ASC01–ASC06) purified scFv antibodies could specifically recognize the ΔhASIC1a nanodiscs, with ASC04 and ASC06 showing the strongest affinities. Immunocytochemistry (ICC) studies show that ASC02, ASC03, ASC04, and ASC06 were able to label the plasma membranes of cells expressing *h*ASIC1a-eYFP, where ASC06 showed the most significant colocalization with *h*ASIC1a-eYFP on the stained membrane (*SI Appendix*, Fig. S1*E*).

The ASC06 antibody was next converted into a full-length IgG1 form (ASC06-IgG1). The yields after purification of ASC06-IgG1 and ASC06 were similar at ~78 mg/L (*SI Appendix*, Fig. S1*F*). To characterize the interaction between ASC06-IgG1 and *h*ASIC1a, the 6H7 stable line expressing the *h*ASIC1a-eYFP fusion protein was used in a Western blot analysis. As shown in *SI Appendix*, Fig. S2*A*, ASC06-IgG1 could not recognize the *h*ASIC1a in the 6H7 lysate by Western blot analysis. By contrast, both the commercial goat polyclonal anti-ASIC1 antibody and the anti-eYFP antibody were able to detect the *h*ASIC1a-eYFP protein in the 6H7 lysate at molecular mass around 100 kDa. We thus reasoned that ASC06-IgG1 recognizes structural epitopes on properly folded and assembled *h*ASIC1a trimer rather than a linear epitope. We next used ASC06-IgG1 to pull down native *h*ASIC1a-YFP in cell lysate followed by anti-eYFP Western blot for *h*ASIC1a-YFP detection. As shown in *SI Appendix*, Fig. S2*B*, a clear band of ~100 kDa representing the *h*ASIC1a-eYFP was observed, indicating that ASC06-IgG1 recognizes *h*ASIC1a in a conformation-dependent manner.

To better understand the nature of the antibody binding, negative staining EM studies were carried out on the ectodomain of *h*ASIC1a (*h*ASIC1a-ECD) and ASC06 in Fab format (ASC06-Fab). Similar to ΔhASIC1a, *h*ASIC1a-ECD exists as homotrimer in solution, which forms stable complex with three ASC06-Fabs (*SI Appendix*, Fig. S3). As the unprocessed negative staining EM image reveals, most of the particles showed a triangular arrangement for the formed complex; meanwhile, particles of boomerang shape and other shapes were also observed, which likely represent complexes with one or two ASC06-Fabs missing (Fig. 1*A*). Then, a total of 5,064 triangular-shaped particles were manually selected from 100 micrographs (Fig. 1*B*) followed by reference-free 2D class averages analyses using the Xmipp CL2D function (Fig. 1*C*). In the 2D averages analyses results, triangular-shaped complexes with clear domain divisions were shown, showing the interactions of ASC06-Fab onto a trimer configuration of *h*ASIC1a-ECD. Combining molecular docking and molecular dynamics simulation, we were able to obtain a model that coarsely reproduces the apparent experimental geometry (Fig. 1*D*). The model predicts that each ASC06-Fab binds to a surface formed by two *h*ASIC1a-ECD subunits, in agreement with the fact that the antibody recognizes *h*ASIC1a in a conformation-dependent manner (Fig. 1*D* and *SI Appendix*, Fig. S2).

Like ASC06, ASC06-IgG1 showed significant membrane colocalization with *h*ASIC1a on the cellular surface (Fig. 2*A*). The binding affinities of ASC06-IgG1 with the purified ΔhASIC1a and the full-length *h*ASIC1a when expressed on a cell surface were then measured using surface plasmon resonance (SPR) and quantitative FACS, respectively. The apparent K_d value of ASC06-IgG1 for the purified ΔhASIC1a is 7.9 nM (*SI Appendix*, Fig. S4*A*). As a positive control, the venom peptide PcTx1 fused with Fc (PcTx1-Fc), showed an apparent K_d of 1.0 nM against the ΔhASIC1a (*SI Appendix*, Fig. S4*B*), consistent with reports in the literature (33).

The interaction between ASC06-IgG1 and the membrane *h*ASIC1a on the 6H7 cells (stable *h*ASIC1a-eYFP expression) was quantitated using a FACS-based assay as shown in Fig. 2*B*. The apparent EC$_{50}$ (concentration for 50% of maximal effect) value was determined to be 2.06 ± 0.01 nM, which is consistent with the
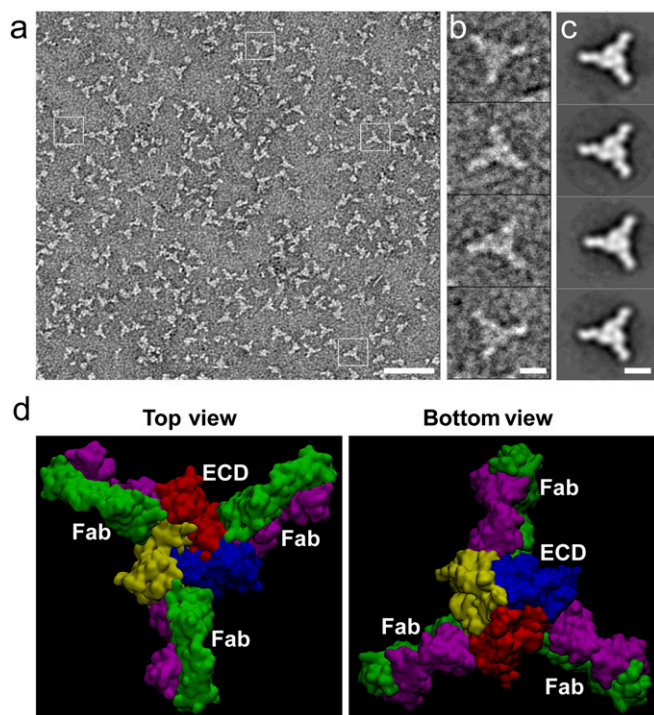
Fig. 1. Negative-staining EM analysis of the *h*ASIC1a-ECD and ASC06-Fab complex. (*A*) Subarea of an unprocessed image of negatively stained *h*ASIC1a-ECD and ASC06-Fab complex. (Scale bar: 50 nm.) (*B*) Representative single particles selected from *A*. (Scale bar: 10 nm.) (*C*) Corresponding representative class averages based on single particles (*n* = 5,064). (Scale bar: 10 nm.) (*D*) Molecular dynamics simulation of the complex from both top and bottom views of the ion channel.

measured K_d value (7.9 nM) against the purified Δ*h*ASIC1a, indicating that the truncated *h*ASIC1a and cell surface-expressed full-length *h*ASIC1a share a similar extracellular conformation.

Binding Selectivity. The sequence homology of ASIC1a between human and rodent is high (>95%), whereas the sequence homology of the ASIC subtypes is low (<50%). The sequence difference between the splicing variants of the same subtype, such as *h*ASIC1a and *h*ASIC1b, is located at the cytoplasmic N terminus and the first transmembrane domain (34). To test the species and subtype selectivity of ASC06-IgG1, we constructed vectors encoding *h*ASIC1b-eYFP fusion, rat acid-sensing ion channel 1a (*r*ASIC1a)-eYFP fusion, mouse acid-sensing ion channel 1a (*m*ASIC1a)-eYFP fusion, *h*ASIC2a-eYFP fusion, *h*ASIC2b-eYFP fusion, and *h*ASIC3a-eYFP fusion. The CHO-K1 cells were transiently transfected with these plasmids. FACS-binding assay and ICC were carried out to determine if ASC06-IgG1 is able to bind to the different ASICs expressed on the cell surface. ICC staining showed membrane colocalization of ASC06-IgG1 with *h*ASIC1a-eYFP, *r*ASIC1a-eYFP, and *m*ASIC1a-eYFP, consistent with the high sequence homology between human and rodent ASIC1a (Fig. 2*A*).

FACS results revealed that ASC06-IgG1 recognized only *h*ASIC1a but not *h*ASIC1b, *h*ASIC2a, *h*ASIC2a/2b, or *h*ASIC3a (Fig. 2*C*), indicating a highly specific subtype selectivity. The binding specificity of ASC06-IgG1 was also shown using the primary cortical neurons from the ASIC1a KO mice (ASIC1a$^{-/-}$). As expected, the primary neurons from the KO mice showed no apparent binding to ASC06-IgG1 in the merged differential interference contrast (DIC) microscope view. When the neurons were transiently transfected with *h*ASIC1a-mCherry, the expression of *h*ASIC1a on the membrane of the neuron was validated and visualized by ASC06-IgG1 (Fig. 2*D*). Furthermore, the am-

plified view of ASC06-IgG1 signal in neuritis showed that the transiently expressed and ASC06-IgG1–labeled *h*ASIC1a was located mainly in the postsynaptic dendrites of neurons (Fig. 2*D*), consistent with the reports in the literature (35).

Functional Characterization of Selected Antibodies. The function of ASC06-IgG1 was characterized by electrophysiology studies of the acid-induced, *h*ASIC1a-mediated electrical current in cells. Decreasing the extracellular pH value (from pH 7.4 to pH 6.0) resulted in the formation of an electric current in the 6H7 stable cell line overexpressing the *h*ASIC1a-eYFP on the membrane (Fig. 3*A*). The amplitudes of the *h*ASIC1a-mediated inward currents of the 6H7 cells were recorded and quantitated in the absence and presence of ASC06-IgG1, with PcTx1 (100 nM) as the positive control (Fig. 3*A*). As shown in Fig. 3 *B* and *C*, ASC06-IgG1 displayed a sustained (30 min) and dose-dependent inhibition of up to 80% of the acid (pH 6.0)-induced currents with an apparent IC_{50} value of 85 ± 6 nM. In contrast, the positive control PcTx1 showed a nearly complete inhibition of the current (Fig. 3 *A* and *C*). Unlike the sustained inhibition with the antibody after washing, the inhibition with PcTx1 could be readily washed out within 5 min (Fig. 3*C*).

To understand the mechanism by which ASC06-IgG1 blocked the *h*ASIC1a currents, SSD and pH activation of *h*ASIC1a in the absence and presence of ASC06-IgG1 were examined. The pH_{50} (a drop in extracellular pH, which can open 50% of the ASIC1a channel) values of the SSD curve and the pH activation curve for *h*ASIC1a were measured and compared with or without 300 nM ASC06-IgG1. As shown in Fig. 3 *D* and *E*, the SSD was induced when applying the conditioning extracellular fluids (ECFs) with different pH values and the activating ECF at pH 6.0, whereas the pH activation curve was constructed when applying the activating ECFs with varying pH values and the conditioning ECF at pH 7.6. No significant differences in the pH_{50} values of SSD and pH activation were observed with 300 nM ASC06-IgG1. In addition, the representative traces of both SSD and activation of ASIC1a currents treated with/without ASC06-IgG1 were displayed in *SI Appendix*, Fig. S5. By contrast, PcTx1 inhibition results in a marked alkaline shift in the curves of SSD and pH activation (36); ASC06-IgG1 seemed to block the activation of the *h*ASIC1a using a mechanism that is noncompetitive with the proton concentration.

The calcium influx of the ASIC1a was measured on a FLIPR instrument using the stable cell line 4C12 expressing *h*ASIC1a-mCherry fusion. In the 4C12 cells, the activation of the homomeric *h*ASIC1a at pH 6.0 at the 10th second of recording seemed to induce a strong calcium influx, whereas the acid-induced calcium influx was not observed for the CHO-K1 cells without *h*ASIC1a expression (*SI Appendix*, Fig. S6*A*). As shown in Fig. 3 *F* and *G*, the *h*ASIC1a-specific antibody, ASC06-IgG1, displayed a dose-dependent inhibition of calcium influx with an IC_{50} of 2.9 ± 0.2 nM. By contrast, the nonselective small molecule ASICs blocker, amiloride, showed only 21% inhibition at 30 μM (*SI Appendix*, Fig. S6).

The Selected Antibody Prevents Acidosis-Induced Cell Death in Vitro. Extracellular acidosis in stroke or ischemia–reperfusion injury is known to induce the activation of ASICs, which leads to neuronal death in the CNS, most likely through transient increase of intracellular calcium and related cell signaling mediated by ASICs (14). The highly potent inhibition of the *h*ASIC1a-mediated calcium influx by ASC06-IgG1 (Fig. 3 *F* and *G*) prompted us to further investigate the protective role of ASC06-IgG1 in acidosis-induced cell death. We began by testing the tolerance of ASC06-IgG1 to acidic conditions. A concentrated ASC06-IgG1 solution (3.3 μM) was incubated at different pH values (from 7.4 to 5.0) for 6 h at 37 °C and subjected to SEC-HPLC analysis. No significant degradation or aggregation of ASC06-IgG1 was observed (*SI Appendix*, Fig. S7). The survival of cells was next assessed by measuring
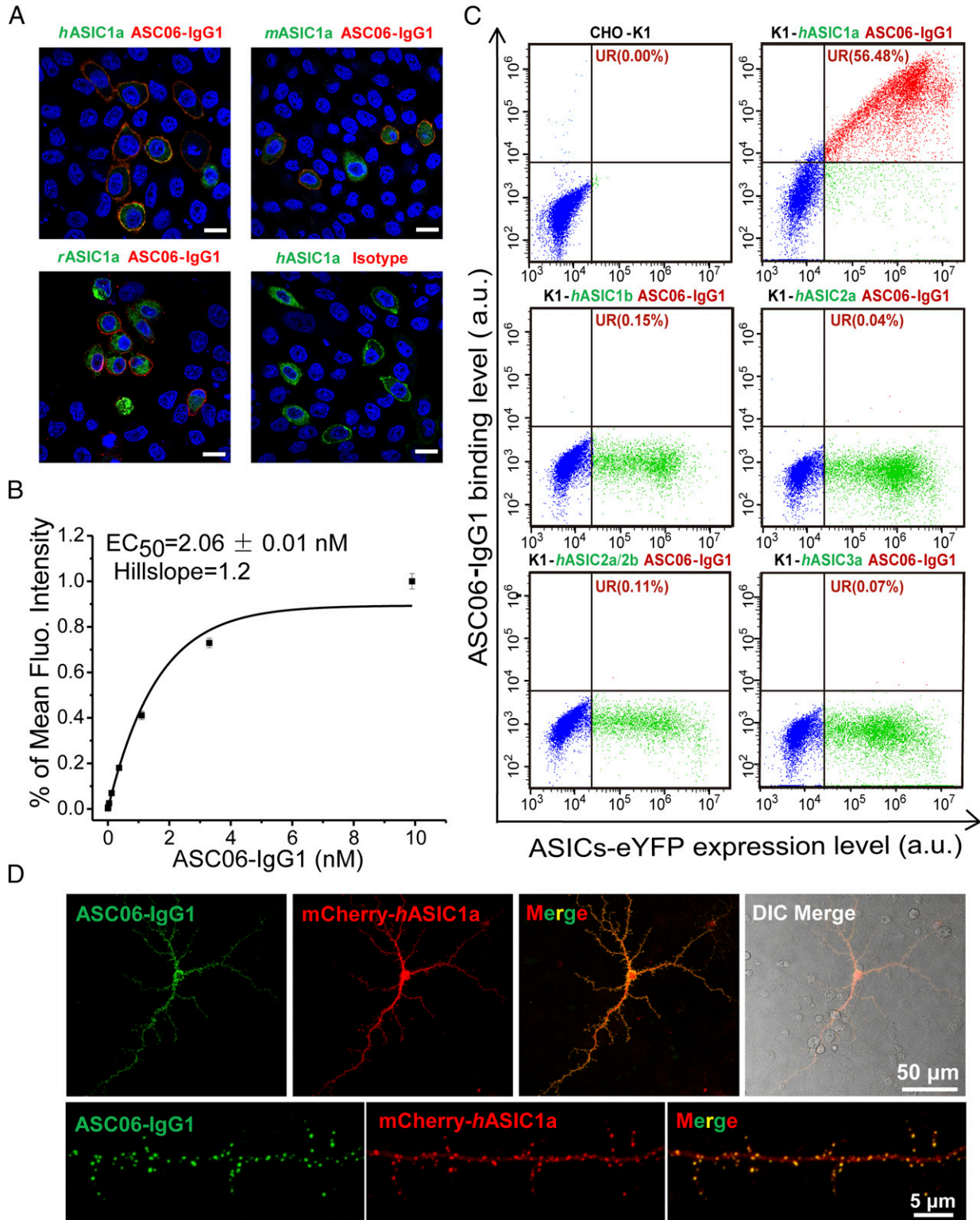
Qiang et al.

www.manaraa.com

Fig. 2. Species and subtype specificities of ASC06-IgG1. (*A*) Confocal images of ASC06-IgG1–labeled CHO-K1 cells (red), which were transiently transfected with *h*ASIC1a-eYFP, *m*ASIC1a-eYFP, and *r*ASIC1a-eYFP (green). DAPI (blue) was used to label the nuclei of cells. (Scale bar: 10 μm.) (*B*) Dose-dependent interaction of ASC06-IgG1 to the 6H7 stable line expressing the *h*ASIC1a-eYFP fusion protein with an apparent EC_{50} value of 2.06 ± 0.01 nM ($n = 3$). (*C*) FACS sorting of the CHO-K1 cells transiently transfected with *h*ASIC1a-eYFP, *h*ASIC1b-eYFP, *h*ASIC2a-eYFP, *h*ASIC2a/2b-eYFP, and *h*ASIC3a-eYFP in the presence of ASC06-IgG1. The association of ASC06-IgG1 with the different subtypes of cell surface *h*ASICs was confirmed by the double-positive cell population constituting eYFP and Alexa555 fluorescences [in the upper right (UR) area of the FACS result; cell number displayed in each plot is 10,000]. (*D*) Confocal images of ASC06-IgG1–labeled primary neurons (green) from cortex of the *m*ASIC1a KO mice sparsely transfected with *h*ASIC1a-mCherry (red). DIC view shows the merged bright field of neurons. *Lower* shows the amplified fields of neuritis indicating that ASC06-IgG1 binding occurs in the postsynaptic dendrites.
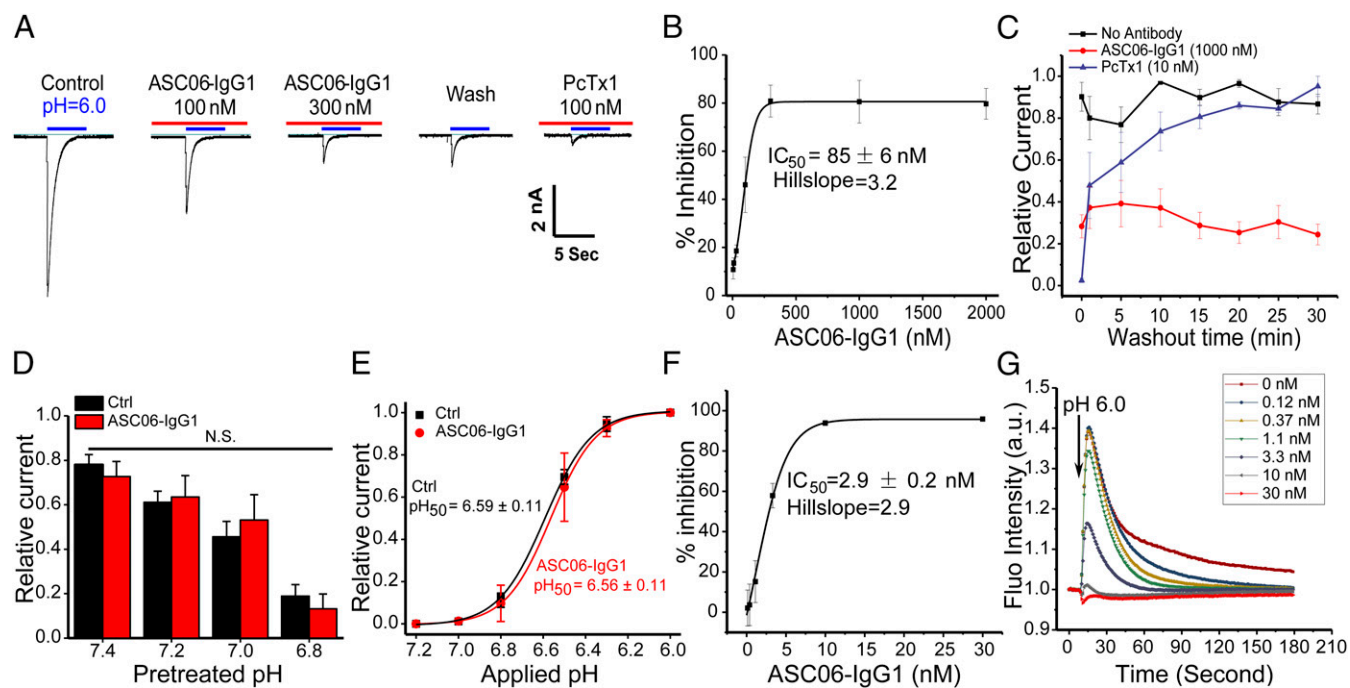
Qiang et al.

www.manaraa.com

Fig. 3. Electrophysiology studies of ASC06-IgG1. Data are shown as mean ± SD of five repeats. (*A*) The representative current traces from one single *h*ASIC1a stable CHO-K1 cell in the absence or presence of different doses of ASC06-IgG1 (100 or 300 nM). PcTx1 acts as a positive control, and "Wash" represents the recovery of the current after the treatment of 300 nM ASC06-IgG1 followed by a 15-min infusion of washing solution. (*B*) Dose-dependent inhibition of ASC06-IgG1 to the acid-induced *h*ASIC1a currents. The apparent IC_{50} value is measured to be 85 ± 6 nM (n = 3–5). (*C*) The washout experiments of ASC06-IgG1 and PcTx1 inactivation of *h*ASIC1a current are shown as the plot of relative currents vs. washout time (minutes; n = 4). (*D*) Effect of ASC06-IgG1 on the SSD profile of the *h*ASIC1a (n = 6–8). (*E*) Effect of ASC06-IgG1 on the proton activation profile of the *h*ASIC1a (n = 5). (*F*) Dose-dependent inhibition of ASC06-IgG1 to the acid-induced calcium influx (n = 6). (*G*) The representative progression curves of the acid-induced calcium influx in the *h*ASIC1a-mCherry–overexpressing stable CHO-K1 cells (4C12) in the presence of various concentrations of ASC06-IgG1 (from 30 to 0.12 nM in 1:3 serial dilutions). Ctrl, currents were measured in absence of ASC06-IgG1; N.S., not significant.

the enzymatic activities of cytoplasmic dehydrogenases and the concentrations of lactate dehydrogenase (LDH) secreted into the cell media, which reflect the cell viability and cytotoxicity, respectively. As shown in Fig. 4 *A* and *B*, the 6H7 stable cell line (bars on the right in Fig. 4 *A* and *B*) showed a higher degree of pH sensitivity than the control CHO-K1 cell, especially at pH 5.5, suggesting that the observed enhanced response to acid was mediated through the *h*ASIC1a on the membrane. Under the same experimental conditions and at pH 5.5, ASC06-IgG1 showed a significant dose-dependent protective effect (Fig. 4 *C* and *D*). In the presence of 1 μM ASC06-IgG1, ~45% of the ASIC1a-expressing stable cells (6H7) survived at pH 5.5 compared with about a 5% survival rate in the absence of the antibody. Consistent with Cell Counting Kit-8 (CCK-8) result, the concentration of LDH released into cell media decreased after the addition of ASC06-IgG1 in a dose-dependent manner (Fig. 4*D*).

The Selected Antibody Protects Brain Cells in Vivo. To determine if the protective effect of antibody ASC06-IgG1 in vitro could be extended to pathologies in vivo, we used the MCAO model to study the antibody's neuroprotective effect. Ischemia was induced by MCAO on the left brain hemisphere of the mice for 60 min before reperfusion. Three hours after ischemia, a total of 4 μL of the vehicle solution (PBS) containing 100 nM PcTx1 or 3.0 μg/μL ASC06-IgG1 was injected intracerebroventricularly (i.c.v.) into the contralateral hemisphere of test mice. An irrelevant antibody (Isotype) with the same concentration of ASC06-IgG1 was administered as a negative control. The infarct volumes of the cortex and striatum were calculated 24 h after the injection (Fig. 5*A*). In the PBS group, ischemia induced a marked infarct in brain (~42% volume compared with the contralateral brain region). PcTx1 markedly decreased the infarct volume to about 17%. Isotype antibody did not

show any protection effect. However, like PcTx1, the group treated with ASC06-IgG1 showed a significantly reduced infarct volume (decrease to about 23%), indicating a potent neuroprotection effect of the antibody against stroke (Fig. 5*B*).

Discussion

The use of combinatorial antibody libraries to generate approved and candidate therapeutic antibodies has seen many iterations (31). Initially, such antibodies were selected against targets where one simply wanted to remove substances from the body regardless of whether they were cancer cells or proteins. For example, some proteins of interest were products of immunological and inflammatory cascades, where it has long been realized that the side effects from an immune response may be harmful. These side effects, often termed the "shrapnel" of the immune response, were initially focused on effector-activating immune complexes but in modern times, concern molecules, such as cytokines and lymphokines. The next iteration involved the generation of functional antibodies, where the antibodies were, for example, agonists that regulated cellular differentiation. Such antibodies bind to cellular receptors and induce the cells to differentiate along normal or alternative pathways (31). Here, we propose a third iteration for the use of therapeutic antibodies based on the realization that, like immune effector proteins, many cells are unable to properly navigate the space between doing good by properly regulating cell physiology and doing harm by overshooting the response. This is especially true in pathological situations. This ability to achieve a properly balanced physiological response is best observed for channels, such as ASIC, where channel opening restores proper physiology, but if the channel remains open too long, cell death can occur. Thus, in strict analogy to the use of antibodies to remove "overshoot" products of immune defense, we amalgamate the
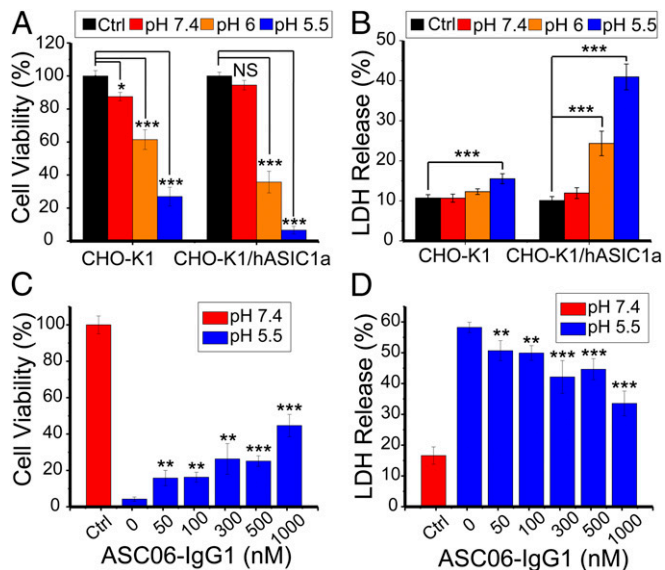
Qiang et al.

Fig. 4. ASC06-IgG1 protects *h*ASIC1a-mediated acidosis-induced cell death. (*A*) Effect of pH (pH 5.5, 6.0, and 7.4) on the viability of CHO-K1 cells with and without the membrane expression of *h*ASIC1a-eYFP measured by the cytoplasmic dehydrogenase activity (*n* = 5–6). (*B*) Effect of pH (pH 5.5, 6.0, and 7.4) on the cytotoxicity of CHO-K1 cell with and without the membrane expression of *h*ASIC1a-eYFP measured by the released LDH activity (*n* = 5–6). (*C* and *D*) Dose-dependent protection of acidosis-induced cell death of the *h*ASIC1a-eYFP stable cells by ASC06-IgG1. Data are shown as mean ± SD of four repeats (*n* = 3–5). NS, not significant. *$P < 0.05$, **$P < 0.01$, ***$P < 0.001$ compared with the control group.

concepts of binding and functional antibodies to regulate cellular processes that might become harmful to the host.

Since the role of calcium influx in the acidosis-induced neuron death has not been well-elucidated, we suspect that the transient increase of cytoplasm calcium induced by the opening of the ASIC1a is a trigger that sets in motion still unknown processes that initiate cell death. The conformational change of the C terminus of ASIC1a was also proposed to be a mechanism for acidosis/ischemia-induced neuron death, which could be an alternative mechanism other than calcium overload (13). The electrophysiological data show that the antibody blocks the ASIC1a in a very efficient manner. There are important differences between our antibodies and the PcTx1 venom peptide. Although the onset of inhibition by the antibody is slower than PcTx1 (it takes about 15 min to reach maximal inhibition), the inhibition effect is longer sustained (even after washout for 30 min, it still has not changed too much). The blocking mechanism also seems to be independent of changing the affinity of protons for channel binding, as preconditioning with the antibody does not alter the SSD (Fig. 3*D* and *SI Appendix*, Fig. S5*A*). Additionally, the channel pH sensitivity is not changed by the antibody (Fig. 3*E* and *SI Appendix*, Fig. S5*B*), which suggests that its mechanism is very different from the classical ASIC1a blocker venom peptide PcTx1. PcTx1 inhibits channel opening by increasing the apparent affinity of the channel for protons, thereby shifting the SSD to higher pH values. For instance, when PcTx1 is used to treat pain, tolerance to the analgesic effects can be developed in a way that resembles repeated morphine injections (37). Since the antibody does not interfere with the apparent proton affinity, we thus speculate that it may block the channel by indirectly affecting the conformational changes of the C terminus of ASIC1a to exert the protection effect (13). However, because the antibody blocks the channel by a totally different mechanism, it could possess unparalleled potential as a therapeutic candidate for the ASIC1a target. Furthermore, it has been reported that *h*ASIC1a has a higher membrane traf-

ficking than *m*ASIC1a, although they share 98% of amino acid identity (38). The exogenous expressed *h*ASIC1a seemed to generate higher currents than *m*ASIC1a, implicating that ASIC1a could play a more important role than what we have learned from rodent mice in human stroke (39). Thus, we are in the process of testing this and other antibodies to different ASICs for their efficacy in the treatment of chronic pain.

Materials and Methods

Reagents and Abbreviations. All of the reagents were purchased from Sigma or as otherwise stated at the highest analytical grades. The recombinant protein symbols are used in the format where an italicized lowercase letter of the initial of species (e.g., human, mouse, rat, etc.) is used as the first letter in the symbol followed by the gene name (e.g., *h*ASIC1a represents the *h*ASIC1a protein). Antibodies were assigned a number arbitrarily by us, like ASC00, according to the panning results. The arbitrary number with or without the "-IgG1" symbol represents the antibody in the format of scFv fused with Fc or full-length IgG1 (IgG1), respectively. All abbreviations are defined at their first occurrence in the paper.

Cell Culture. The CHO-K1 cell line (#CRL-9618; ATCC) was maintained in an F-12k media (#21127022; Gibco) containing 10% (vol/vol) FBS (#1600074; Gibco), whereas the FreeStyle 293F (#R79007; ThermoFisher Scientific) cell line was cultured in a Freestyle 293 expression media (#12338026; Thermo-Fisher Scientific). *Spodoptera frugiperda* 9 (Sf9) cells (#12659017; Thermo-Fisher Scientific) was cultured at 27 °C in an ESF921 media (#96–001-01; Expression Systems). Primary cortical neurons dissected from E18-d-old C57 BL/6 mice or ASIC1a$^{-/-}$ mice were maintained in a Neurobasal media (#21103049; Gibco) supplemented with B27 (#17504044; Gibco) and Glutamx I (#35050061; Gibco).

The CHO-K1/*h*ASIC1a stable cell line overexpressing the full-length *h*ASIC1a (1–528 amino acids) channel was generated as follows. The cDNA of the full-length *h*ASIC1a with a C-terminal eYFP fusion or a C-terminal mCherry fusion was constructed, cloned into a pCDNA3.1-Neo–expressing vector, and transfected into the CHO-K1 cells using Lipofectin 2000. The CHO-K1/*h*ASIC1a stable cell line was selected by the antibiotic, geneticin (up to 1 mg/mL), and validated by the fused fluorescence proteins eYFP (λ_{ex} = 488 nm; λ_{em} = 528 nm) and mCherry fluorescence (λ_{ex} = 587 nm; λ_{em} = 610 nm) using flow cytometry. In the presence of 200 μg/mL geneticin, over 80% positive cells survived when cultured for 30 d. The clonal stable lines were sorted out using a flow cytometry instrument (BD FACSAria III) based
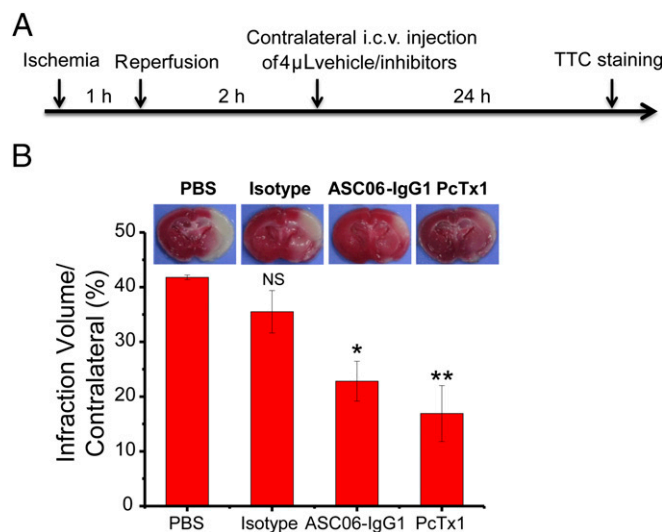

Fig. 5. MCAO model studies. (*A*) Schematic diagram of the in vivo experimental design. (*B*) TTC-stained brain sections showing infarct area (images) and volume (bar graph) in brains from PBS-treated (sham control, *n* = 6), isotype control-treated (*n* = 6), ASC06-IgG1–treated (*n* = 6), and PcTx1-treated (*n* = 6) mice. (Magnification: *B*, *Upper*, 0.9×.) NS, not significant. *P value < 0.05 compared with the sham control group; **P value < 0.01 compared with the sham control group.

on the expression of eYFP (6H7 cell line) and mCherry (4C12 cell line) and expanded using an F-12K media supplemented with 10% (vol/vol) FBS and 200 μg/mL geneticin. The hASIC1a-specific monoclonal antibody, ASC06, was used to further confirm the overexpression of hASIC1a.

Purification of Recombinant Truncated hASIC1a. The cDNA encoding the truncated hASIC1a sequence (amino acids 13–464; hereafter referred to as ΔhASIC1a) and an N-terminal Flag-tag were cloned into a pEG BacMam expression vector (courtesy of Eric Gouaux, Howard Hughes Medical Institute, Oregon Health and Science University, Portland, OR). The ΔhASIC1a protein was then heterologously expressed in the HEK293F cells using the BacMam system as reported (40). In brief, the pEG BacMam-ΔhASIC1a construct was generated and transformed into the DH10Bac Escherichia coli cells (ΔhASIC1a bacmids). The resulting bacmids were then transfected into the Sf9 cells using the FuGENE transfection reagent (Promega) to obtain the P3 baculovirus (amplified twice). The HEK293F cells (2×10^6 cells per 1 mL) were infected by the baculovirus at a volume ratio of 1:25 (virus:cell) for 24 h at 37 °C. The infected cells were incubated in the presence of 2 mM sodium butyrate at 37 °C for 48 h to boost the expression of the target protein. Cells were harvested by centrifugation at $2,000 \times g$ per 1 min.

All of the following procedures were carried out on ice unless specified otherwise. Cell pellets from a 2 L biomass were first resuspended in a 100 mL hypotonic buffer (10 mM Tris, pH 7.5, 10 mM MgCl$_2$, 20 mM KCl) supplemented with the protease inhibitor mixture (one tablet per 50 mL; Roche), grounded with a tissue dounce homogenizer, and centrifuged at $80,000 \times g$ for 40 min. After repeating the process once, the resulting pellets were resuspended in 100 mL of a higher osmotic buffer (10 mM Tris, pH 7.5, 10 mM MgCl$_2$, 20 mM KCl, 1 M NaCl), homogenized, and centrifuged. This procedure was also repeated one more time. The resulting pellets were then mixed and treated with 2 mg/mL iodoacetamide in a 50 mL hypotonic buffer containing protease inhibitors for 30 min. The recombinant ΔhASIC1a protein was extracted in a cell lysis buffer [100 mM Tris, pH 7.5, 1.6 M NaCl, 1% n-dodecyl b-D-maltopyranoside (DDM), 0.2% cholesteryl hemisuccinate (CHS)] under gentle agitation at 4 °C for 3 h. After 30 min of centrifugation at $15,000 \times g$, supernatant was incubated with the anti-FLAG M2 magnetic beads (#M8823; Sigma) overnight under gentle agitation. The magnetic beads were washed once each with buffer A (50 mM Tris, pH 7.5, 800 mM NaCl, 10% glycerol, 0.1% DDM, 0.02% CHS, 10 mM MgCl$_2$) and buffer B (25 mM Tris, pH 7.5, 800 mM NaCl, 10% glycerol, 0.05% DDM, 0.01% CHS). The ΔhASIC1a protein was eluted using the buffer B supplemented with 0.1 mg/mL Flag peptide, concentrated, further purified using the SEC on a Superdex 200 column (GE Heathcare), and concentrated to yield 60 μL of 15 mg/mL stock solution of homogeneous ΔhASIC1a with purity >90% as judged by SDS/PAGE analysis (SI Appendix, Fig. S1A).

Nanodisc Assembly of hASIC1a Channel. To mimic the lipid bilayer environment of cellular membranes, the purified ΔhASIC1a protein was incorporated into a lipid nanodisc by mixing the ΔhASIC1a protein with the MSP1 and 1,2-dimyristoyl-sn-glycero-3-phosphocholine (DMPC) at a molar ratio of 3:2:65. The associated detergents were removed by gentle agitation with the Bio-Beads SM2 [Bio-Beads:DDM = 10:1 (wt/wt); Bio-Rad] overnight. The ΔhASIC1a-embedded nanodisc assembly was separated from the unassembled ones using the Flag peptide-specific magnetic beads (41). The desired ΔhASIC1a nanodisc assembly was further purified and collected using a Superose 6 column (GE Heathcare) in a buffer containing 20 mM Tris, pH 7.5, and 150 mM NaCl. The empty nanodiscs were packaged without the addition of ΔhASIC1a. The composition of the assembled ΔhASIC1a nanodiscs was analyzed by SDS/PAGE, EM, and dynamic light scattering.

Differential Enrichment-Based Screening of Combinatorial Antibody Library. The hASIC1a-specific scFv antibodies were selected from a combinatorial human monoclonal scFv antibody phage library (10^{11} diversity) after three rounds of affinity enrichment against the biotinylated ΔhASIC1a nanodiscs immobilized on the streptavidin-coated magnetic beads (#21925; Pierce). The phage antibody library panning followed a modified procedure as described previously (42). Briefly, phagemids (displaying the antibody library) binding to the antigen (ΔhASIC1a nanodiscs) were enriched at each cycle and eluted with Glycine-HCl (pH 2.2). The XL1-Blue cells were used to express and amplify the output phagemids for the next rounds of panning. To minimize nonspecific enrichment, a differential enrichment phage display selection was used, in which excessive amounts of the empty nanodiscs (two times above the amount of ΔhASIC1a nanodiscs) were used to pull down the nonspecific phagemids before panning against the ΔhASIC1a nanodiscs in the second and third cycles. After three iterations, 96 positive colonies were selected and analyzed by phage ELISA as described (42). All of the positive clones were se-

quenced. Both the DNA and protein sequences of CDR3 domains were analyzed using the international ImMunoGeneTics information platform. A phylogenetic tree was constructed after aligning of the CDR3 sequences. Six distinctive scFv sequences were highly enriched.

Expression and Purification of Antibodies. Genes encoding the candidate scFv sequences were cloned into a modified pFUSE expression vector (#pfuse-hg1fc2; Invivogen) to obtain the scFv-Fc fusion protein constituting the entire Fc domain of human IgG1. For the full-length IgG1 antibody, variable regions of heavy chain and light chain from the scFv vector were cloned to plasmids with intact constant heavy-chain domain and intact constant light-chain domain, respectively. The HEK293F cells transfected with the scFv-Fc vectors or cotransfected with equal molar of heavy-chain vectors and light-chain vectors were cultured for 4 d. After centrifugation, the scFv-Fc or full-length IgG1 antibodies secreted into the media were purified using a HiTrap Protein A HP column (#17–0403-03; GE Healthcare) with a citrate elution buffer, pH 3.4, on an ÄKTA purifier 100 (GE Healthcare). The purified antibodies (SI Appendix, Fig. S1F) were then concentrated (15 mg/mL) and stored in a PBS buffer, pH 7.4, at −80 °C.

Negative Stain EM: Sample Preparation and Data Collection. The antigen-binding fragment of ASC06-IgG1 (ASC06-Fab) was prepared by digesting ASC06-IgG1 with papain followed by protein A affinity purification and gel filtration. The ectodomain of hASIC1a (hASIC1a-ECD) with an N-terminal fused IL-2 tag and Flag tag was expressed in HEK293F cells and purified by anti-Flag M2 magnetic beads and gel filtration using PBS buffer, pH 7.4. The ASC06-Fab and hASIC1a-ECD were incubated at a molar ratio of 3:1 in PBS buffer, pH 7.4, overnight at 4 °C to form a tertiary complex. This complex was further isolated by gel filtration, and the peak fractions containing this complex were collected and subjected to negative staining EM.

The EM samples were prepared by diluting the purified complex of hASIC1a-ECD and ASC06-Fab to 0.01 mg/mL. Then, 4-μL sample droplets were absorbed for 1 min on freshly glow-discharged copper grids covered by a thin and continuous carbon film (#BZ31024a; Beijing Zhongjingkeyi Technology). The grids were washed with two drops of deionized water, subsequently negatively stained with two drops of 0.75% (wt/vol) uranyl formate (#22450; Electron Microscopy Sciences) for 1 min before blotting with filter papers, and then, air dried.

All micrographs were recorded with a Tecnai G2 Spirit transmission electron microscope (FEI) equipped with an LaB$_6$ cathode operated at 120 kV and a $4,000 \times 4,000$ Eagle CCD camera at a calibrated magnification of 67,000 times, resulting in a pixel size of 1.74 Å.

EM Image Processing and 3D Reconstruction. The Scipion software suite (43) was used for all image processing steps. All of the recorded micrographs were first decimated twofold (resulting in a pixel size of 3.48 Å). Then, a total of 5,064 particles were manually selected from 100 micrographs with the EMAN2 Boxer function (44) using a box size of 96×96 pixels. Reference-free 2D class averages analyses was generated using the Xmipp CL2D function (45).

Molecular Dynamics Simulation. The models for the hASIC1a and for the ASC06 in Fab format were derived by homology by using the Swiss Model website (46). The template for ASIC1a proteins was obtained from the structure of the truncated chicken protein [Protein Data Bank (PDB) ID code 4FZ0]. To compare the negative staining results with a possible atomistic model, we first generate a series of different possible dockings of the Fab to the ECD of the hASIC1a (only residues 73–425 were kept) using the ClusPro 2.0 server (47) and the antibody docking mode (48). We then subselected eight of them with geometry that was more compatible with the one described by the negative staining and performed energy minimization followed by 20-ns molecular dynamics simulation to relax the interaction and stabilize the structure of the complex. After this procedure, only one model seemed to satisfy the overall geometry that is experimentally observed in negative staining experiments. Simulations were performed using the Gromacs 4.6.7 package (49) and the Amber14ffSB force field (50). All of the systems were solvated with full-atom TIP3P water containing Cl$^-$ and K$^+$ ions at a concentration of ~0.15 M to mimic a physiological ionic strength. Temperature T and pressure P were kept constant at 300 K and 1 atm, respectively, using the Berendsen thermostat and barostat (51). Fast smooth Particle-Mesh Ewald summation (52) was used for long-range electrostatic interactions, with a cutoff of 1.0 nm for the direct interactions.

The model of ASIC1a inserted in the nanodisc used to generate SI Appendix, Fig. S1 was obtained starting from the crystal structure of

MSP1 protein (PDB ID code 2MSC) in complex with the ASIC1a trimer and filled with 91 DMPC molecules.

ELISAs. Avidin (#21121; Pierce) was diluted to a final concentration of 2 ng/μL in the Carbonate–Bicarbonate buffer (#C3041; Sigma). The resulting avidin solution was used to coat the 96-well plates (25 μL per well) at 4 °C overnight. The coated plates were washed once with the 0.05% Tween-20–containing phosphate buffered solution (PBST) buffer (150 μL per well) followed by the addition and incubation of 25 μL biotinylated ΔhASIC1a nanodisc solution (2 ng/μL) in each well at 37 °C for 1 h. The PBST buffer alone and the empty nanodisc solution (2 ng/μL) were used as the background and negative controls, respectively. After removal of the incubation solution, the resulting plates were rinsed once using the PBST buffer and incubated with a blocking solution containing 5% (vol/vol) milk in PBST (150 μL per well) at 37 °C for 1 h. After blocking and PBST washing (one time), 25 μL of the scFv-Fc antibody solution [10 μg/mL in PBST containing 1% (vol/vol) milk] was added to each well and incubated at 37 °C for 1 h. The resulting plates were rinsed eight times using PBST before subjecting to HRP detection. A solution containing the goat anti-human Fc HRP-conjugated secondary antibody (dilution factor 1:5,000; #A0170; Sigma) and the anti-M13 HRP-conjugated secondary antibody (dilution factor 1:5,000; #27–9421-01; GE/Amersham/Whatman) was added into the above plates (50 μL per well) and incubated at 37 °C for 1 h. The plates were then washed eight times with PBST followed by the addition of 50 μL 2,2′-azinobis [3-ethylbenzothiazoline-6-sulfonic acid]-diammonium salt solution (#11684302001; Roche) into each well. After 20 min of incubation at room temperature, the absorption changes at 405 nm in each well were measured on a microplate reader (Enspire; PerkinElmer).

Affinity Determination. SPR and flow cytometry methods were used to study the interaction between the monoclonal antibody and hASIC1a. SPR-binding studies were performed on a Biacore T200 (GE Healthcare). The anti-Flag antibody was amine coupled to the surface of a biosensor chip CM5 series S (GE Healthcare). The recombinant Flag-tagged ΔhASIC1a was then immobilized onto the chip surface. Serially diluted antibody ASC06-IgG1 (1, 5, 10, 50, 100 nM) was applied in a running buffer (pH 7.4) containing 25 mM Hepes, 500 mM NaCl, 0.05% EDTA, and 0.05% DDM. The kinetics of binding/dissociation was measured as a change in the SPR signal resonance units. Apparent binding constants were calculated using the Biacore T200 evaluation software with a single-cycle kinetic model.

In the flow cytometry-binding experiments, ASIC1a-eYFP–expressing stable cells (6H7) were collected and resuspended in ice cold FACS buffer (PBS, 0.05% BSA, 2 mM EDTA). Equal amounts of 6H7 cells (50,000 cells per tube) were then incubated with different concentrations of ASC06-IgG1 for 20 min at 4 °C, washed with 1 mL ice cold FACS buffer, spun, and resuspended in 100 μL ice cold FACS buffer containing the Alexa555-conjugated secondary antibody that recognizes human Fc [1:800 (vol/vol) dilution; Life Technology]. After incubating at 4 °C for 15 min, the cells were washed twice and resuspended in the FACS buffer, and then, they were sorted and analyzed on a flow cytometer (CytoFLEX S; Beckman Culter) to determine relative binding level by the antibodies to the stable cell lines overexpressing hASIC1a. Mean fluorescent intensities of Alexa555 in eYFP-positive cells were recorded and analyzed to calculate the apparent binding affinity of antibody.

Cell Membrane Colocalization Studies Using ICC. Cells (CHO-K1) were seeded onto the poly-D-lysine–coated glass bottom 24-well plates at a concentration of 2×10^5 cells per 1 mL. After 12 h of cultivation, the CHO-K1 cells were transfected with ASICs plasmids by Lipofectin 3000 reagent. Twenty-four hours after transfection, the cells were fixed in 4% paraformaldehyde and incubated for 30 min in a blocking solution (5% goat serum in PBS). The resulting cells were incubated with 2 μg/mL ASC06-IgG1 at 4 °C overnight followed by three PBS washes for 5 min each and incubation with the Alexa555-conjugated goat anti-human secondary antibody (Life Technology). After three additional PBS washes for 5 min each, the nuclei of the cells were stained with DAPI (#10236276001; Roche). The ICC analysis was performed on a laser scanning confocal microscopy (ZEISS LSM710) with a 63×/N.A. 1.4 objective at 25 °C. Images were collected on a 1,024 × 1,024-pixel EM-CCD camera. Data acquisition and analyses were performed with the ZEN 2012 professional software.

Electrophysiological Experiments. The inward cellular ASIC1a current was recorded from a single cell using standard whole-cell recording techniques by a patch-clamp amplifier (Axon 200B; Axon Instruments). Membrane currents were sampled and analyzed using a Digidata 1320A interface and a personal computer with Clampex and Clampfit software (Version 9.0.1; Axon Instru-

ments). For a typical experiment, an ECF containing 150 mM NaCl, 5 mM KCl, 10 mM Hepes, 10 mM D-glucose, 2 mM CaCl₂, and 1.0 mM MgCl₂ with the osmotic pressure in the range of 320–335 mOsm was adjusted to pH 7.4 with 5 M NaOH. Patch electrodes (4–6 MΩ) contained 30 mM NaCl, 120 mM KCl, 0.5 mM CaCl₂, 1 mM MgCl₂, 10 mM Hepes, 2 mM MgATP, and 5 mM EGTA (pH 7.2; adjusted with 5 M KOH) at 300 mOsm. The ASIC1a activating ECF is identical to the normal ECF, except that MES was used to replace Hepes to maintain the ECF at pH 6.0. A coverslip with discretely distributed individual CHO-ASIC1a stable cells (6H7) on the surface was placed into a recording chamber under a constant perfusion (~2–3 mL/min) generated by an ALA 8 channel perfusion system (ALA Scientific Instruments Inc.) mounted on an inverted microscope. After achieving the break-in (whole-cell) configuration, the cell was voltage clamped at a holding potential of −70 mV. The normal ECF (pH 7.4) was first perfused onto the patched cell, and then, the activating ECF of pH 6.0 was rapidly applied to elicit a maximum inward ASIC1a current as control current. When testing the inhibition effect of the antibody, ECFs of pH 7.4 containing different concentrations of ASC06-IgG1 were perfused from low to high concentration into the recording chamber for 10–15 min. To measure the inhibition of the current, the activating ECFs of pH 6.0 containing the corresponding concentrations of the testing antibodies were applied to the same patched 6H7 cell to generate the inward currents that can be normalized to the control current of the same cell. The small molecule inhibitor amiloride (#S1811; Selleck) and the venom peptide PcTx1 (#4435s; Peptide Institute) at concentrations of 30 μM and 100 nM, respectively, were used as the positive controls for the inhibition of the ASIC1a current. Data acquired from four to five cells were used for statistical calculation of inhibition effects.

For the measurement of SSD, the pH of the conditioning ECF was adjusted to 7.6, 7.4, 7.2, 7.0, and 6.8 (in a Hepes buffer), while the activating ECF was maintained at pH 6.0 (in an MES buffer). For the measurement of pH activation of the hASIC1a in the 6H7 stable cells, the conditioning ECF was fixed at pH 7.6 (in a Hepes buffer), and the pH of the activating ECF was adjusted to 7.4, 7.2, 7.0, 6.8, 6.5, 6.3, and 6.0. The hASIC1a currents were recorded when the stable cell line 6H7 was patched in the presence and absence of 300 nM ASC06-IgG1. The relative currents expressed as fractions of the maximum amplitude on the sensorgram (I/I_{max}) were calculated and plotted to constitute SSD and pH activation profiles. Each data point represents the average of at least five patched cells.

Calcium Influx. The FLIPR Calcium 5 Assay kit was used to determine the acid-induced calcium influx in the hASIC1a-mCherry–expressing stable CHO-K1 cells (4C12). Cells were seeded in a clear bottom 96-well plate at a density of 10,000 per well 24 h before assay. Assay buffer and dye loading buffer (1.26 mM CaCl₂, 0.5 mM MgCl₂, 0.4 mM MgSO₄, 5.33 mM KCl, 0.44 mM KH₂PO₄, 4.17 mM NaHCO₃, 138 mM NaCl, 0.338 mM Na₂HPO₄, 20 mM Hepes, pH 7.4) were prepared according to the manufacturer's instruction. Probenecid was added to the dye loading buffer to a final concentration of 2.5 mM immediately before use. Fifty microliters of the assay buffer containing ASC06-IgG1 was incubated with the 4C12 cells for 30 min at 37 °C before an equal volume of the dye loading buffer was added. Amiloride as well as PcTx1 and an isotype antibody were used as the positive and negative controls, respectively. Cells were incubated with the dye loading buffer for 1 h before reading on an FDSS/μCELL plate reader (Hamamatsu); 100 μL of the pH 6.0 activation buffer (same composition with assay buffer; pH was adjusted to 6.0) was added to the cells at a speed of 50 μL/s. The progression curve of the calcium signal produced in each well was recorded continuously for 10 s before the addition of the activation buffer (preread) and 170 s after the addition on an FDSS/μCELL (excitation wavelength: 480 nm; emission wavelength: 540 nm) FLIPR reader. To determine the IC₅₀ value of ASC06-IgG1 in the inhibition of ASIC1a-mediated current, a 1:3 serial dilution of ASC06-IgG1 was applied to the 4C12 cells with six repeats for each concentration.

Acidosis-Induced Cell Death. The hASIC1a-eYFP stable cells (6H7) and CHO-K1 cells were seeded in a 96-well plate at a density of 10,000 cells per well 1 d before treatment. ECF solutions at pH 5.5, 6.0, and 7.4 were used to treat the cells at 37 °C for 6 h. To test the rescuing effect of ASC06-IgG1, the antibody was dissolved in an acidic ECF (pH 5.5) to make the final antibody concentrations of 0, 50, 100, 300, 500, and 1,000 nM. The 6H7 cells were first preincubated with the antibody at the corresponding concentrations at 37 °C for 30 min in cell media. After replacing the cell media with the corresponding acidic ECFs, the cells were incubated at 37 °C for 6 h, washed with a PBS buffer (pH 7.4), and then cultured in a 1% FBS DMEM/F-12K media overnight. The supernatants of the overnight culture were collected for the LDH release measurement using a LDH Assay kit (#88953; Thermo Fisher Scientific). The cells viability was determined using the CCK-8 assay kit (#CK04; Dojindo).

Qiang et al.

www.manaraa.com

MCAO Model. Animal care and the experimental protocols were approved by the Animal Ethics Committee of Shanghai Jiao Tong University School of Medicine, Shanghai, China. A transient ischemic stroke in the left brain hemisphere was established in male mice (C57 BL/6, 20–25 g) using the MCAO model for 1 h before reperfusion. Three hours after ischemia, a total of 4 μL of vehicle solution (PBS) in the absence or presence of neuroprotective agents [100 nM PcTx1 and 3.0 μg/μL endotoxin-free ASC06-IgG1 (20 μM)] was injected i.c.v. on the contralateral side of the brain hemisphere. An irrelevant endotoxin-free antibody (3.0 μg/μL, 20 μM) was used as isotype control. The cerebral blood flow was monitored by transcranical LASER Doppler to ensure that the ischemia was successfully induced. Mice were killed 24 h after i.c.v. injection. Mice brains were rapidly dissected and sectioned transversely into serial intervals slices followed by staining with a 2% vital dye 2,3,5-triphenyltetrazolium hydrochloride (TTC). The infarct area was calculated by subtracting the normal area stained with TTC in the ischemic hemisphere from that of the nonischemic hemisphere. The infarct volume was calculated by summing infarction areas of all sections and multiplying by slice thickness.

Data Analysis. The results were expressed as means ± SD unless otherwise indicated. Data analysis was performed by one-way ANOVA using OriginPro 2017 statistical software. Significance was assumed at the P value <0.05.

Data Availability. Data will be available from the corresponding authors on request.

1. Waldmann R, Champigny G, Bassilana F, Heurteaux C, Lazdunski M (1997) A proton-gated cation channel involved in acid-sensing. *Nature* 386:173–177.
2. Kellenberger S, Schild L (2015) International Union of Basic and Clinical Pharmacology. XCI. structure, function, and pharmacology of acid-sensing ion channels and the epithelial Na+ channel. *Pharmacol Rev* 67:1–35.
3. Jasti J, Furukawa H, Gonzales EB, Gouaux E (2007) Structure of acid-sensing ion channel 1 at 1.9 A resolution and low pH. *Nature* 449:316–323.
4. Wemmie JA, Taugher RJ, Kreple CJ (2013) Acid-sensing ion channels in pain and disease. *Nat Rev Neurosci* 14:461–471.
5. Rash LD (2017) Acid-sensing ion channel pharmacology, past, present, and future.... *Adv Pharmacol* 79:35–66.
6. Chesler M (2003) Regulation and modulation of pH in the brain. *Physiol Rev* 83:1183–1221.
7. Wang YZ, Xu TL (2011) Acidosis, acid-sensing ion channels, and neuronal cell death. *Mol Neurobiol* 44:350–358.
8. Wemmie JA, et al. (2002) The acid-activated ion channel ASIC contributes to synaptic plasticity, learning, and memory. *Neuron* 34:463–477.
9. Li WG, et al. (2016) ASIC1a regulates insular long-term depression and is required for the extinction of conditioned taste aversion. *Nat Commun* 7:13770.
10. Kreple CJ, et al. (2014) Acid-sensing ion channels contribute to synaptic transmission and inhibit cocaine-evoked plasticity. *Nat Neurosci* 17:1083–1091.
11. Xiong ZG, et al. (2004) Neuroprotection in ischemia: Blocking calcium-permeable acid-sensing ion channels. *Cell* 118:687–698.
12. Gao J, et al. (2005) Coupling between NMDA receptor and acid-sensing ion channel contributes to ischemic neuronal death. *Neuron* 48:635–646.
13. Wang YZ, et al. (2015) Tissue acidosis induces neuronal necroptosis via ASIC1a channel independent of its ionic conduction. *eLife* 4:e05682, and erratum (2016) 5:e14128.
14. Yermolaieva O, Leonard AS, Schnizler MK, Abboud FM, Welsh MJ (2004) Extracellular acidosis increases neuronal cell calcium by activating acid-sensing ion channel 1a. *Proc Natl Acad Sci USA* 101:6752–6757.
15. Chu XP, Xiong ZG (2013) Acid-sensing ion channels in pathological conditions. *Adv Exp Med Biol* 961:419–431.
16. Baron A, Lingueglia E (2015) Pharmacology of acid-sensing ion channels–Physiological and therapeutical perspectives. *Neuropharmacology* 94:19–35.
17. Li MH, Inoue K, Si HF, Xiong ZG (2011) Calcium-permeable ion channels involved in glutamate receptor-independent ischemic brain injury. *Acta Pharmacol Sin* 32:734–740.
18. Xu TL, Xiong ZG (2007) Dynamic regulation of acid-sensing ion channels by extracellular and intracellular modulators. *Curr Med Chem* 14:1753–1763.
19. Kellenberger S, Schild L (2002) Epithelial sodium channel/degenerin family of ion channels: A variety of functions for a shared structure. *Physiol Rev* 82:735–767.
20. Voilley N, de Weille J, Mamet J, Lazdunski M (2001) Nonsteroid anti-inflammatory drugs inhibit both the activity and the inflammation-induced expression of acid-sensing ion channels in nociceptors. *J Neurosci* 21:8026–8033.
21. Lynagh T, Romero-Rojo JL, Lund C, Pless SA (2017) Molecular basis for allosteric inhibition of acid-sensing ion channel 1a by ibuprofen. *J Med Chem* 60:8192–8200.
22. Vick JS, Askwith CC (2015) ASICs and neuropeptides. *Neuropharmacology* 94:36–41.
23. Duan B, et al. (2011) Extracellular spermine exacerbates ischemic neuronal injury through sensitization of ASIC1a channels to extracellular acidosis. *J Neurosci* 31:2101–2112.
24. Babini E, Paukert M, Geisler HS, Grunder S (2002) Alternative splicing and interaction with di- and polyvalent cations control the dynamic range of acid-sensing ion channel 1 (ASIC1). *J Biol Chem* 277:41597–41603.
25. Escoubas P, et al. (2000) Isolation of a tarantula toxin specific for a class of proton-gated Na+ channels. *J Biol Chem* 275:25116–25121.
26. Diochot S, et al. (2004) A new sea anemone peptide, APETx2, inhibits ASIC3, a major acid-sensitive channel in sensory neurons. *EMBO J* 23:1516–1525.
27. Diochot S, et al. (2012) Black mamba venom peptides target acid-sensing ion channels to abolish pain. *Nature* 490:552–555.
28. Bohlen CJ, et al. (2011) A heteromeric Texas coral snake toxin targets acid-sensing ion channels to produce pain. *Nature* 479:410–414.
29. Chassagnon IR, et al. (2017) Potent neuroprotection after stroke afforded by a double-knot spider-venom peptide that inhibits acid-sensing ion channel 1a. *Proc Natl Acad Sci USA* 114:3750–3755.
30. Huse WD, et al. (1989) Generation of a large combinatorial library of the immunoglobulin repertoire in phage lambda. *Science* 246:1275–1281.
31. Lerner RA (2016) Combinatorial antibody libraries: New advances, new immunological insights. *Nat Rev Immunol* 16:498–508.
32. McCafferty J, Griffiths AD, Winter G, Chiswell DJ (1990) Phage antibodies: Filamentous phage displaying antibody variable domains. *Nature* 348:552–554.
33. Dawson RJ, et al. (2012) Structure of the acid-sensing ion channel 1 in complex with the gating modifier psalmotoxin 1. *Nat Commun* 3:936.
34. Hoagland EN, Sherwood TW, Lee KG, Walker CJ, Askwith CC (2010) Identification of a calcium permeable human acid-sensing ion channel 1 transcript variant. *J Biol Chem* 285:41852–41862.
35. Wemmie JA, et al. (2003) Acid-sensing ion channel 1 is localized in brain regions with high synaptic density and contributes to fear conditioning. *J Neurosci* 23:5496–5502.
36. Chen X, Kalbacher H, Gründer S (2005) The tarantula toxin psalmotoxin 1 inhibits acid-sensing ion channel (ASIC) 1a by increasing its apparent H+ affinity. *J Gen Physiol* 126:71–79.
37. Mazzuca M, et al. (2007) A tarantula peptide against pain via ASIC1a channels and opioid mechanisms. *Nat Neurosci* 10:943–945.
38. Xu Y, et al. (2018) Human ASIC1a mediates stronger acid-induced responses as compared with mouse ASIC1a. *FASEB J* 32:3832–3843.
39. Jing L, et al. (2012) N-glycosylation of acid-sensing ion channel 1a regulates its trafficking and acidosis-induced spine remodeling. *J Neurosci* 32:4080–4091.
40. Goehring A, et al. (2014) Screening and large-scale expression of membrane proteins in mammalian cells for structural studies. *Nat Protoc* 9:2574–2585.
41. D'Antona AM, Xie G, Sligar SG, Oprian DD (2014) Assembly of an activated rhodopsin-transducin complex in nanoscale lipid bilayers. *Biochemistry* 53:127–134.
42. Xu L, et al. (2017) Design and characterization of a human monoclonal antibody that modulates mutant connexin 26 hemichannels implicated in deafness and skin disorders. *Front Mol Neurosci* 10:298.
43. de la Rosa-Trevín JM, et al. (2016) Scipion: A software framework toward integration, reproducibility and validation in 3D electron microscopy. *J Struct Biol* 195:93–99.
44. Tang G, et al. (2007) EMAN2: An extensible image processing suite for electron microscopy. *J Struct Biol* 157:38–46.
45. de la Rosa-Trevín JM, et al. (2013) Xmipp 3.0: An improved software suite for image processing in electron microscopy. *J Struct Biol* 184:321–328.
46. Biasini M, et al. (2014) SWISS-MODEL: Modelling protein tertiary and quaternary structure using evolutionary information. *Nucleic Acids Res* 42:W252–W258.
47. Comeau SR, Gatchell DW, Vajda S, Camacho CJ (2004) ClusPro: A fully automated algorithm for protein-protein docking. *Nucleic Acids Res* 32:W96–W99.
48. Brenke R, et al. (2012) Application of asymmetric statistical potentials to antibody-protein docking. *Bioinformatics* 28:2608–2614.
49. Pronk S, et al. (2013) GROMACS 4.5: A high-throughput and highly parallel open source molecular simulation toolkit. *Bioinformatics* 29:845–854.
50. Lindorff-Larsen K, et al. (2010) Improved side-chain torsion potentials for the Amber ff99SB protein force field. *Proteins* 78:1950–1958.
51. Berendsen HJC, Postma JPM, van Gunsteren WF, DiNola A, Haak JR (1984) Molecular dynamics with coupling to an external bath. *J Chem Phys* 81:3684–3690.
52. Darden T, York D, Pedersen L (1993) Particle mesh Ewald: An N·log(N) method for Ewald sums in large systems. *J Chem Phys* 98:10089–10093.

APPLIED BIOLOGICAL SCIENCES

Qiang et al.

www.manaraa.com